Contribution from the Lehrstuhl für Anorganische Chemie I der Ruhr-Universität, D-4630 Bochum, FRG, Anorganisch-Chemisches Institut der Universität, D-6900 Heidelberg, FRG, and Institut für Physik, Medizinische Universität, D-2400 Lübeck, FRG

A New Tetranuclear Oxohydroxoiron(III) Cluster: Crystal Structure, Magnetic Properties, and EXAFS Investigation of $[L_4Fe_4(\mu\text{-}O)_2(\mu\text{-}OH)_4]I_4\cdot 3H_2O$ (L = 1,4,7-Triazacyclononane)

Stefan Drüeke,[1a] Karl Wieghardt,*[,1a] Bernhard Nuber,[1b] Johannes Weiss,[1b] Emile L. Bominaar,[1c] A. Sawaryn,[1c] H. Winkler,[1c] and A. X. Trautwein[1c]

Received January 17, 1989

Hydrolysis of the cation $[L_2Fe_2(acac)_2(\mu\text{-}O)]^{2+}$ in aqueous solution yields the new tetranuclear species $[L_4Fe_4(\mu\text{-}O)_2(\mu\text{-}OH)_4]^{4+}$, where L represents the cyclic amine 1,4,7-triazacyclononane (L; $C_6H_{15}N_3$) and acac is acetylacetonate(1−). The green tetraiodide trihydrate and the tetraperchlorate trihydrate have been isolated as solid materials. The crystal structure of $[L_4Fe_4(\mu\text{-}O)_2(\mu\text{-}OH)_4]I_4\cdot 3H_2O$ has been determined by X-ray crystallography. Crystal data: monoclinic; $P2_1/a$ (C_{2h}^5); a = 14.653 (6) Å; b = 19.092 (7) Å; c = 17.309 (8) Å; β = 91.80 (3)°; V = 4839.9 Å^3; Z = 4. Four ferric ions are connected by two μ_2-oxo and four μ_2-hydroxo bridges, forming the distorted adamantane-like core $[Fe_4(\mu\text{-}O)_2(\mu\text{-}OH)_4]^{4+}$; each Fe^{III} center is capped by the tridentate amine L (*fac*-FeN_3O_3 donor set at each Fe^{III}). The complex may be envisaged as a dimer of the dimer containing a $[Fe\text{–}O\text{–}Fe]^{4+}$ core. From temperature-dependent susceptibility measurements strong intramolecular antiferromagnetic coupling between all four high-spin ferric ions is established (S = 0 ground state; J = −106.3 (2) cm^{-1} and J' = −15.1 (2) cm^{-1}). EXAFS spectra of the tetraiodide and of the tetraperchlorate are in excellent agreement with the results obtained by crystallography: in particular, the two different intramolecular Fe···Fe distances at 3.33 and 3.53 Å and the differing Fe–O_{oxo} and Fe–$O_{hydroxo}$ distances at 1.82 and 2.00 Å, respectively, are clearly detected in both salts. In alkaline solution the tetranuclear complex is shown to dissociate, generating most probably two of the binuclear species $[LFe(OH)_2(\mu\text{-}O)Fe(OH)_2L]$. The process is reversible; reacidification regenerates the tetranuclear complex.

Introduction

In recent years a steadily increasing number of oxo/hydroxo-bridged clusters of iron(III) have been synthesized and structurally characterized. Complexes of nuclearity Fe_3, Fe_4, Fe_6, Fe_8 and Fe_{11} have been isolated, and their spectroscopic and magnetic properties have been investigated in considerable detail.[2] Interest in this chemistry has been stimulated by the fascinating problem of the uptake and release of iron in the iron storage protein ferritin.[3] Other non-heme, iron-containing metalloproteins such as hemerythrin[4] and a ribonucleotide reductase[5] have been shown to contain binuclear $[Fe\text{–}O\text{–}Fe]^{4+}$ units in the active sites.

We have recently reported the facile hydrolysis of the binuclear complex $[L_2Fe_2(\mu\text{-}O)(acac)_2]^{2+}$ in aqueous solution, where L represents the macrocycle 1,4,7-triazacyclononane and acac is the monoanion acetylacetonate(1−).[6] In the presence of NaX salts (X = I^-, ClO_4^-, PF_6^-) green microcrystals with an L:Fe:X ratio of 1:1:1 precipitated. From their magnetic properties it was concluded that the tetranuclear cation $[L_4Fe_4(\mu\text{-}O)_2(\mu\text{-}OH)_4]^{4+}$ formed. At that time single crystals suitable for X-ray crystallography were not obtained. Here we report the crystal structure of $[L_4Fe_4(\mu\text{-}O)_2(\mu\text{-}OH)_4]I_4\cdot 3H_2O$, green crystals of which were obtained from the above reaction mixture in the presence of excess NaI.

There have been six crystallographically characterized tetranuclear iron(III) clusters described in the literature that contain μ_2-oxo, μ_3-oxo, μ_2-hydroxo, and/or μ_2-alkoxo bridges and, in addition, bridging carboxylato or carbonato ligands: $[Et_4N][Fe_4(\mu_3\text{-}O)_2(O_2CR)_7(H_2Bpz_2)_2]$;[7] $[Fe_4(\mu_3\text{-}O)_2(bicoH)_2(bico)_2(O_2CPh)_4]Cl_2$;[8] $[Fe_4(\mu_3\text{-}O)_2(O_2CCF_3)_8(H_2O)_6]\cdot 2H_2O$;[9] $(pyrrH)_4[Fe_4(\mu_2\text{-}O)_2(\mu_2\text{-}OH)_2(5\text{-}Me\text{-}hxta)_2]\cdot 2CH_3OH$;[10] $Na_6[Fe_4(\mu_2\text{-}O)_2(CO_3)_2L'_2]$;[11a] $[Fe_4O_2L_2(OBz)_2](ClO_4)_2(OTs)_2$.[11b] The first three of these may be envisaged as dimers of dimers—at least formally—with formation of μ_3-oxo bridges from μ_2-oxo-bridged dimers:

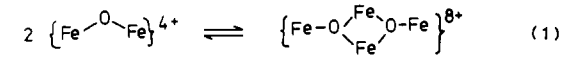

(1)

On the other hand, Que's compound $(pyrrH)_4[Fe_4(\mu_2\text{-}O)_2(\mu\text{-}OH)_2(5\text{-}Me\text{-}hxta)_2]\cdot 2CH_3OH$[10] may also be viewed as a dimer of dimers but without formation of μ_3-oxo bridges (5-Me-hxta represents the deprotonated form of *N*,*N*′-2-hydroxy-5-methyl-1,3-xylylenebis[*N*-(carboxymethyl)glycine]). Here the dimerization reaction has been shown to occur in solution:

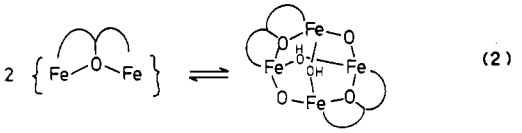

(2)

Two phenoxo, two oxo, and two hydroxo bridges form a distorted adamantane-like $[Fe_4(\mu_2\text{-}OR)_2(\mu_2\text{-}OH)_2(\mu_2\text{-}O)_2]^{4+}$ core.

Table I. Crystallographic Data for $[L_4Fe_4(O)_2(OH)_4]I_4\cdot 3H_2O$

chem formula	$[(C_6H_{15}N_3)_4Fe_4O_2\text{-}(OH)_4]I_4\cdot 3H_2O$	Z	4
fw	1401.9	λ	Mo Kα (graphite monochromated)
space group	$P2_1/a$ (C_{2h}^5)	ρ(calcd), g cm^{-3}	1.92
T, °C	22	μ, cm^{-1}	37.52
a, Å	14.653 (6)	transmission coeff	0.51–1.00
b, Å	19.092 (7)	$R(F_o)$	0.057
c, Å	17.309 (8)	$R_w(F_o^2)$	0.052 ($w = 1/\sigma^2(F)$)
β, deg	91.80 (3)		
V, Å^3	4839.9		

(1) (a) Ruhr-Universität Bochum. (b) Universität Heidelberg. (c) Medizinische Universität Lübeck.
(2) Lippard, S. J. *Angew. Chem., Int. Ed. Engl.* **1988**, *27*, 353 and references cited therein; *Chem. Br.* **1986**, 222.
(3) (a) Clegg, G. A.; Fitton, J. E.; Harrison, P. M.; Treffry, A. *Prog. Biophys. Mol. Biol.* **1988**, *36*, 53. (b) Crichton, R. R. *Angew. Chem., Int. Ed. Engl.* **1973**, *12*, 57. (c) Theil, E. C. *Annu. Rev. Biochem.* **1987**, *56*, 289.
(4) (a) Kurtz, D. M.; Shriver, D. F.; Klotz, I. M. *Coord. Chem. Rev.* **1977**, *24*, 145. (b) Wilkins, P. C.; Wilkins, R. G. *Coord. Chem. Rev.* **1987**, *79*, 195.
(5) (a) Sjöberg, B.-M.; Loehr, T. M.; Sanders-Loehr, J. *Biochemistry* **1982**, *21*, 96. (b) Petersson, A.; Gräslund, A.; Ehrenberg, A.; Sjöberg, B.-M.; Reichard, P. *J. Biol. Chem.* **1980**, *255*, 6706.
(6) Wieghardt, K.; Pohl, K.; Bossek, U.; Nuber, B.; Weiss, J. *Z. Naturforsch.* **1988**, *43B*, 1184.
(7) Armstrong, W. H.; Roth, M. E.; Lippard, S. J. *J. Am. Chem. Soc.* **1987**, *109*, 6318.
(8) Gorun, S. M.; Lippard, S. J. *Inorg. Chem.* **1988**, *27*, 149.
(9) Ponomarev, V. I.; Atovmyan, L. O.; Bobkova, S. A.; Turtê, K. I. *Dokl. Akad. Nauk SSSR* **1984**, *274*, 368.
(10) (a) Murch, B. P.; Boyle, P. D.; Que, L., Jr. *J. Am. Chem. Soc.* **1985**, *107*, 6728. (b) Murch, B. P.; Bradley, F. C.; Boyle, P. D.; Papaefthymiou, V.; Que, L., Jr. *J. Am. Chem. Soc.* **1987**, *109*, 7993.
(11) (a) Jameson, D. L.; Xie, C.-L.; Hendrickson, D. N.; Potenza, J. A.; Schugar, H. J. *J. Am. Chem. Soc.* **1987**, *109*, 740. (b) Chen, Q.; Lynch, J. B.; Gomez-Romero, P.; Ben-Hussein, A.; Jameson, G. B.; O'Connor, C. J.; Que, L., Jr. *Inorg. Chem.* **1988**, *27*, 2673.

0020-1669/89/1328-4477$01.50/0

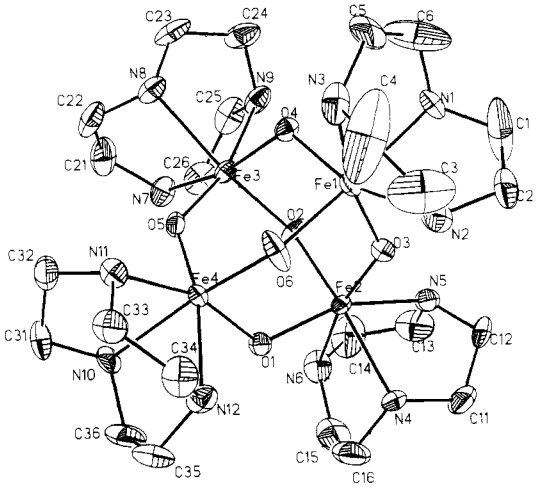

Figure 1. Perspective view of the cation in $[L_4Fe_4(\mu\text{-}O)_2(\mu\text{-}OH)_4]I_4\cdot 3H_2O$ and atom-labeling scheme.

The reaction described in this work does not involve carboxylate, carbonate, or any other chelating ligand with additional, potentially bridging oxygen functionalities. The acac ligands in $[L_2Fe_2(\mu_2\text{-}O)(acac)_2]^{2+}$ are labile in aqueous solution.[6] They are readily displaced by water (or hydroxide), forming a binuclear intermediate that dimerizes in neutral or slightly alkaline solution, generating $[L_4Fe_4(\mu\text{-}O)_2(\mu\text{-}OH)_4]^{4+}$. The core $[Fe_4(\mu_2\text{-}O)_2(\mu_2\text{-}OH)_4]^{4+}$ has also an adamantane-like structure. Thus, our complex and Que's are members of the same family of complexes. The behavior in solution and the magnetic properties of this new tetranuclear species are described here. In addition, we have measured the EXAFS spectra of the iodide and perchlorate salt.

Results and Discussion

Crystal Structure. The structure of the cation in $[L_4Fe_4(O)_2(OH)_4]I_4\cdot 3H_2O$ is shown in Figure 1. Four iron(III) centers, each of which is coordinated to a tridentate macrocycle, are connected by two μ_2-oxo and four μ_2-hydroxo bridges forming the distorted adamantane-like core $[Fe_4(\mu\text{-}O)_2(\mu\text{-}OH)_4]^{4+}$. This core can alternatively be viewed as a dimer of the well-known binuclear $[Fe\text{-}O\text{-}Fe]^{4+}$ structural unit, two of which are linked by four hydroxo bridges.

Although the positions of the hydrogen atoms of the OH bridges have not been located, they are readily identified by comparing the respective Fe–O bond distances within the $[Fe_4(O)_2(OH)_4]^{4+}$ core (Table III). Four short $Fe\text{–}O_{oxo}$ bonds are identified (average 1.816 Å); they are well in the range 1.76–1.82 Å observed for all crystallographically characterized $[Fe\text{–}O\text{–}Fe]^{4+}$ units.[2] Thus, oxygen atoms O(3) and O(5) are oxo bridges. The $Fe\text{–}O_{hydroxo}$ bond lengths are significantly longer (average 1.997 Å). The difference $d(Fe\text{–}O_{hydroxo}) - d(Fe\text{–}O_{oxo})$ of 0.181 Å is significantly larger than 3 times the estimated standard deviations of these bond lengths (σ = 0.007 Å). Therefore, oxygen atoms O(1), O(2), O(4), and O(6) are considered to be hydroxo bridges. This assignment agrees well with the difference reported for the pair of complexes $[(HB(pz)_3)_2Fe_2(\mu\text{-}O)(\mu\text{-}CH_3CO_2)_2]$ and $[(HB(pz)_3)_2Fe_2(OH)(CH_3CO_2)_2]^+$.[12] Furthermore, a small but significant structural trans influence of the oxo bridges is observed that is not present for hydroxo bridges. The $Fe\text{–}N_{trans}$ bonds in trans positions with respect to the $Fe\text{–}O_{oxo}$ bonds are longer by 0.048 Å than the corresponding $Fe\text{–}N_{cis}$ bonds (which are in trans positions with respect to the $Fe\text{–}O_{hydroxo}$ bonds).

Interestingly, the Fe–O–Fe bond angles involving oxo and hydroxo bridges are also distinctly different (Table IV): The $Fe\text{–}O_{hydroxo}\text{–}Fe$ angles range from 123.7 to 125.4°, whereas the corresponding angles at the two oxo bridges are 132.8 and 132.5°.

(12) (a) Armstrong, W. H.; Lippard, S. J. *J. Am. Chem. Soc.* **1983**, *105*, 4837. Armstrong, W. H.; Spool, A.; Papefthymiou, G. C.; Frankel, R. B.; Lippard, S. J. *J. Am. Chem. Soc.* **1984**, *106*, 3653. (b) Armstrong, W. H.; Lippard, S. J. *J. Am. Chem. Soc.* **1984**, *106*, 4632.

Table II. Atom Coordinates ($\times 10^4$) for $[L_4Fe_4(O)_2(OH)_4]I_4\cdot 3H_2O$

atom	x	y	z
I(1)	9380 (1)	6849 (1)	4508 (1)
I(2)	3502 (1)	5540 (1)	2629 (1)
I(3)	9101 (1)	6370 (1)	438 (1)
I(4)	8844 (1)	2425 (1)	2200 (1)
Fe(1)	7120 (1)	5922 (1)	2417 (1)
Fe(2)	7293 (1)	4483 (1)	1346 (1)
Fe(3)	7197 (1)	4303 (1)	3377 (1)
Fe(4)	9126 (1)	4876 (1)	2639 (1)
O(1)	8579 (4)	4397 (3)	1709 (3)
O(2)	6799 (4)	4042 (3)	2300 (3)
O(3)	6929 (4)	5366 (3)	1575 (3)
O(4)	6816 (4)	5304 (3)	3295 (3)
O(5)	8416 (4)	4452 (3)	3345 (3)
O(6)	8487 (4)	5788 (3)	2476 (4)
N(1)	5749 (5)	6381 (4)	2445 (4)
N(2)	7223 (6)	6842 (4)	1653 (4)
N(3)	7298 (6)	6840 (4)	3223 (5)
C(1)	5573 (8)	6789 (8)	1775 (8)
C(2)	6285 (9)	6991 (8)	1338 (7)
C(3)	7681 (11)	7427 (6)	2042 (7)
C(4)	7757 (13)	7401 (7)	2816 (9)
C(5)	6407 (10)	7017 (8)	3535 (7)
C(6)	5623 (9)	6787 (7)	3130 (8)
N(4)	7802 (5)	4713 (5)	186 (4)
N(5)	6060 (5)	4341 (4)	594 (4)
N(6)	7446 (6)	3409 (4)	851 (5)
C(11)	7062 (7)	4831 (7)	−386 (5)
C(12)	6155 (7)	4885 (7)	−27 (5)
C(13)	5912 (8)	3616 (7)	337 (6)
C(14)	6520 (9)	3115 (6)	764 (7)
C(15)	7966 (10)	3408 (8)	142 (7)
C(16)	8399 (8)	4100 (8)	2 (7)
N(7)	7361 (5)	3188 (4)	3675 (4)
N(8)	7255 (5)	4324 (4)	4651 (4)
N(9)	5779 (5)	3982 (4)	3721 (4)
C(21)	7658 (8)	3079 (6)	4476 (6)
C(22)	7893 (7)	3777 (6)	4878 (5)
C(23)	6348 (8)	4263 (6)	5003 (5)
C(24)	5588 (7)	4370 (6)	4418 (5)
C(25)	5706 (7)	3217 (6)	3797 (6)
C(26)	6504 (7)	2847 (5)	3463 (6)
N(10)	10181 (5)	4036 (4)	2757 (4)
N(11)	10098 (4)	5334 (4)	3473 (4)
N(12)	10254 (5)	5245 (4)	1881 (4)
C(31)	10785 (7)	4154 (5)	3442 (5)
C(32)	10446 (7)	4734 (5)	3943 (5)
C(33)	10837 (6)	5742 (5)	3128 (5)
C(34)	10653 (7)	5871 (5)	2291 (6)
C(35)	10943 (7)	4697 (6)	1752 (6)
C(36)	10684 (7)	4013 (6)	2027 (6)
Wa(1)	4849 (5)	4209 (4)	1967 (4)
Wa(2)	7416 (6)	5870 (4)	4897 (4)
Wa(3)	3300 (6)	3922 (5)	3639 (5)

Table III. Bond Lengths (Å)

Fe(1)–O(3)	1.818 (6)	Fe(1)–O(4)	1.986 (5)
Fe(1)–O(6)	2.020 (6)	Fe(1)–N(1)	2.193 (7)
Fe(1)–N(2)	2.207 (8)	Fe(1)–N(3)	2.250 (8)
Fe(2)–O(1)	1.974 (5)	Fe(2)–O(2)	2.008 (5)
Fe(2)–O(3)	1.815 (6)	Fe(2)–N(4)	2.209 (7)
Fe(2)–N(5)	2.210 (7)	Fe(2)–N(6)	2.237 (8)
Fe(3)–O(2)	2.000 (5)	Fe(3)–O(4)	1.994 (5)
Fe(3)–O(5)	1.810 (5)	Fe(3)–N(7)	2.202 (7)
Fe(3)–N(8)	2.203 (6)	Fe(3)–N(9)	2.265 (8)
Fe(4)–O(1)	1.999 (6)	Fe(4)–O(5)	1.820 (5)
Fe(4)–O(6)	1.992 (6)	Fe(4)–N(10)	2.232 (7)
Fe(4)–N(11)	2.178 (7)	Fe(4)–N(12)	2.255 (7)
Fe(3)···Fe(1)	3.509 (3)	Fe(4)···Fe(1)	3.565 (3)
Fe(2)···Fe(1)	3.328 (3)	Fe(4)···Fe(2)	3.523 (3)
Fe(3)···Fe(2)	3.539 (3)	Fe(4)···Fe(3)	3.323 (3)

The iron–iron separations across the oxo bridges are 3.328 (2) and 3.323 (3) Å, whereas the average of the four iron–iron separations across the hydroxo bridges is 3.534 Å. The structural features described here for the $[Fe_4(\mu\text{-}O)_2(\mu\text{-}OH)_4]^{4+}$ core are very similar to those described by Que et al. for $(pyrrH)_4[Fe_4$-

Table IV. Bond Angles (deg)

O(3)-Fe(1)-O(4)	103.5 (2)	O(3)-Fe(1)-O(6)	95.4 (3)
O(4)-Fe(1)-O(6)	97.5 (3)	O(3)-Fe(1)-N(1)	97.7 (3)
O(4)-Fe(1)-N(1)	89.6 (3)	O(6)-Fe(1)-N(1)	163.2 (3)
O(3)-Fe(1)-N(2)	89.8 (3)	O(4)-Fe(1)-N(2)	162.4 (3)
O(6)-Fe(1)-N(2)	92.6 (3)	N(1)-Fe(1)-N(2)	77.0 (3)
O(3)-Fe(1)-N(3)	164.6 (3)	O(4)-Fe(1)-N(3)	90.7 (3)
O(6)-Fe(1)-N(3)	88.3 (3)	N(1)-Fe(1)-N(3)	76.4 (3)
N(2)-Fe(1)-N(3)	75.1 (3)	O(1)-Fe(2)-O(2)	94.0 (2)
O(1)-Fe(2)-O(3)	107.0 (3)	O(2)-Fe(2)-O(3)	95.4 (2)
O(1)-Fe(2)-N(4)	87.7 (2)	O(2)-Fe(2)-N(4)	166.3 (3)
O(3)-Fe(2)-N(4)	97.1 (3)	O(1)-Fe(2)-N(5)	158.7 (3)
O(2)-Fe(2)-N(5)	97.1 (2)	O(3)-Fe(2)-N(5)	90.1 (3)
N(4)-Fe(2)-N(5)	77.4 (3)	O(1)-Fe(2)-N(6)	86.5 (3)
O(2)-Fe(2)-N(6)	88.5 (3)	O(3)-Fe(2)-N(6)	165.6 (3)
N(4)-Fe(2)-N(6)	78.0 (3)	N(5)-Fe(2)-N(6)	75.6 (3)
O(2)-Fe(3)-O(4)	95.7 (2)	O(2)-Fe(3)-O(5)	105.7 (2)
O(4)-Fe(3)-O(5)	97.0 (2)	O(2)-Fe(3)-N(7)	90.2 (2)
O(4)-Fe(3)-N(7)	166.2 (3)	O(5)-Fe(3)-N(7)	93.3 (3)
O(2)-Fe(3)-N(8)	159.7 (3)	O(4)-Fe(3)-N(8)	93.2 (3)
O(5)-Fe(3)-N(8)	91.2 (3)	N(7)-Fe(3)-N(8)	77.4 (3)
O(2)-Fe(3)-N(9)	86.2 (2)	O(4)-Fe(3)-N(9)	91.2 (3)
O(5)-Fe(3)-N(9)	164.7 (2)	N(7)-Fe(3)-N(9)	76.7 (3)
N(8)-Fe(3)-N(9)	75.4 (3)	O(1)-Fe(4)-O(5)	96.5 (2)
O(1)-Fe(4)-O(6)	96.4 (3)	O(5)-Fe(4)-O(6)	102.0 (3)
O(1)-Fe(4)-N(10)	90.2 (2)	O(5)-Fe(4)-N(10)	91.6 (3)
O(6)-Fe(4)-N(10)	164.1 (3)	O(1)-Fe(4)-N(11)	162.8 (2)
O(5)-Fe(4)-N(11)	96.3 (2)	O(6)-Fe(4)-N(11)	92.1 (3)
N(10)-Fe(4)-N(11)	78.0 (3)	O(1)-Fe(4)-N(12)	87.5 (2)
O(5)-Fe(4)-N(12)	167.1 (3)	O(6)-Fe(4)-N(12)	89.7 (3)
N(10)-Fe(4)-N(12)	76.1 (3)	N(11)-Fe(4)-N(12)	77.6 (3)
Fe(2)-O(1)-Fe(4)	125.0 (3)	Fe(2)-O(2)-Fe(3)	124.0 (3)
Fe(1)-O(3)-Fe(2)	132.8 (3)	Fe(1)-O(4)-Fe(3)	123.7 (3)
Fe(3)-O(5)-Fe(4)	132.5 (3)	Fe(1)-O(6)-Fe(4)	125.4 (3)

Table V. Hydrogen Bonding in $[L_4Fe_4(O)_2(OH)_4]I_4 \cdot 3H_2O$

I(1)···N(3)	3.718 (6)	I(2)···Wa(1)	3.437 (8)
I(1)···N(11)	3.577 (7)	I(2)···Wa(3)	3.567 (8)
I(1)···Wa(2)	3.514 (8)	I(3)···N(2)	3.630 (7)
I(4)···N(6)	3.589 (8)	I(3)···N(12)	3.668 (7)
I(4)···N(7)	3.704 (7)	Wa(2)···Wa(3)	2.800 (7)
Wa(1)···N(5)	3.020 (6)	Wa(2)···N(8)	2.991 (8)

$(HXTA)_2O_2(OH)_2]$, where the adamantane-like core consists of two oxo, two hydroxo, and two phenoxo bridges.[10]

The geometry around each iron is the same for all four ferric ions; a distorted-octahedral, facial FeN_3O_3 environment is observed. Due to the steric constraints of the coordinated amine, the N-Fe-N bond angles are significantly smaller (average 76.7°) than the octahedral angle of 90° (Table IV). This has been observed for many complexes of iron(III) containing the coordinated 1,4,7-triazacyclononane ligand.[13]

Three of the four iodide anions in crystals of $[L_4Fe_4(O)_2(OH)_4]I_4 \cdot 3H_2O$ form N-H···I contacts to the amine groups of the macrocyclic ligands of the cation (Table V): they are each bound to two such groups from two different macrocycles of one cation. Iodide I(2) is not bound to any secondary amine protons; instead, it is bound to two water molecules of crystallization. In addition, one O-H···O bond between Wa(2) and Wa(3) is found and there are a number of N-H···O contacts between secondary amine protons and water molecules of crystallization.

EXAFS Spectroscopy. We have recorded the X-ray absorption spectra of $[L_4Fe_4(\mu\text{-}O)_2(\mu\text{-}OH)_2]I_4 \cdot 3H_2O$ and of the tetraperchlorate around the iron K edge. The reason for doing this was the following. We had previously synthesized and crystallographically characterized the complex $[L_4Mn_4(\mu\text{-}O)_6]Br_4 \cdot 5.5H_2O$, which was shown to contain a symmetric adamantane-like $[Mn_4O_6]^{4+}$ core.[14] This core had been proposed as a possible

Table VI. Results of Final EXAFS Fit Including Five Shells[a]

	compd I	compd II
threshhold energy E_0, eV	13.11 ± 0.25	12.30 ± 0.51
dist, Å		
R_1	3.300 ± 0.036	3.361 ± 0.028
R_2	3.531 ± 0.006	3.549 ± 0.006
R_3	1.802 ± 0.008	1.817 ± 0.013
R_4	1.993 ± 0.005	2.005 ± 0.007
R_5	2.195 ± 0.009	2.215 ± 0.009
Debye-Waller factors, Å^2		
σ_1	0.023 ± 0.009	0.023 ± 0.007
σ_2	0.006 ± 0.001	0.007 ± 0.001
σ_3	0.001 ± 0.001	0.009 ± 0.003
σ_4	0.001 ± 0.001	0.005 ± 0.001
σ_5	0.010 ± 0.002	0.010 ± 0.002
fit index (FI)[28]	5.41	2.51

[a] Definitions: R_1, σ_1, Fe-Fe (O bridge); R_2, σ_2, Fe-Fe (OH bridge); R_3, σ_3, Fe-O (O bridge); R_4, σ_4, Fe-O (OH bridge); R_5, σ_5, Fe-N; I, $[L_4Fe_4(\mu\text{-}O)_2(\mu\text{-}OH)_4]I_4 \cdot 3H_2O$; II, $[L_4Fe_4(\mu\text{-}O)_2(\mu\text{-}OH)_4](ClO_4)_4 \cdot 3H_2O$; FI = $\{1/[100(NPT)]\}\sum_{i=1}^{NPT}[(\chi_{calcd} - \chi_{exptl})k^{wt}]^2$; NPT = number of data points; wt = weight factor (1.0); χ_{calcd}, χ_{exptl} = absorption coefficients; k = wavenumber.

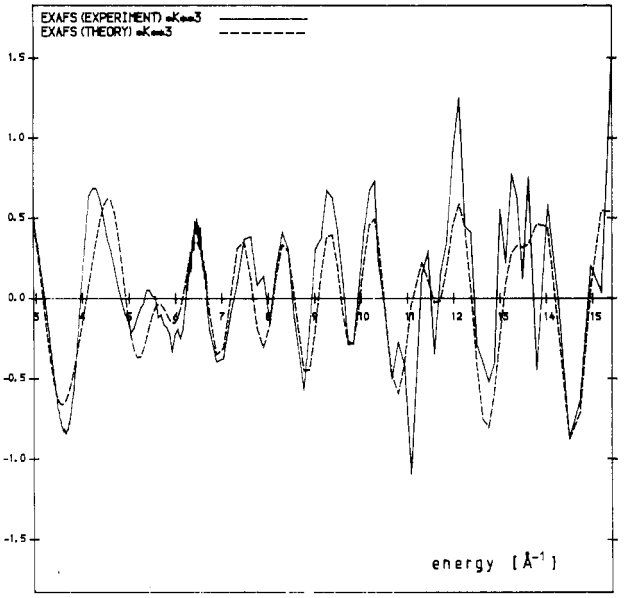

Figure 2. Experimental EXAFS spectrum for $[L_4Fe_4(\mu\text{-}O)_2(\mu\text{-}OH)_4]I_4 \cdot 3H_2O$ and fit curve obtained with the parameters listed in Table VI. The deviation of experiment and theory is due to the fact that the theoretical spectrum represents the two regions 1.45-2.2 and 3.1-3.9 Å of the Fourier transform only.

structure of the active site in the water-oxidizing apparatus of photosystem II (PS II).[15] It is believed to contain four manganese centers, two of which are in rather close proximity (Mn···Mn ≈ 2.7 Å) as was shown by detailed EXAFS investigations by Klein[16] and by Cramer.[17] The above low-molecular-weight manganese complex has been investigated by EXAFS spectroscopy as a model compound for PS II.[18] It was concluded that an adamantane-like $[Mn_4O_6]^{4+}$ core is *not* a likely candidate for the structure of the active site in PS II; it is too symmetrical. Therefore, it appeared interesting to investigate an *unsymmetrical* adamantane core and

(13) (a) Wieghardt, K.; Pohl, K.; Gebert, W. *Angew. Chem.* **1983**, *95*, 739; *Angew. Chem., Int. Ed. Engl.* **1983**, *22*, 727. (b) Spool, A.; Williams, I. D.; Lippard, S. J. *Inorg. Chem.* **1985**, *24*, 2156.
(14) (a) Wieghardt, K.; Bossek, U.; Gebert, W. *Angew. Chem.* **1983**, *95*, 320; *Angew. Chem., Int. Ed. Engl.* **1983**, *22*, 328. (b) Wieghardt, K.; Bossek, U.; Nuber, B.; Weiss, J.; Bonvoisin, J.; Corbella, M.; Vitols, S. E.; Girerd, J. J. *J. Am. Chem. Soc.* **1988**, *110*, 7398.
(15) Brudvig, G. W.; Crabtree, R. H. *Proc. Natl. Acad. Sci. U.S.A.* **1986**, *83*, 4586.
(16) (a) Kirby, J. A.; Robertson, A. S.; Smith, J. P.; Thompson, A. C.; Cooper, S. R.; Klein, M. P. *J. Am. Chem. Soc.* **1981**, *103*, 5529. (b) Kirby, J. A.; Goodin, D. B.; Wydrzynski, T.; Robertson, A. S.; Klein, M. P. *J. Am. Chem. Soc.* **1981**, *103*, 5537. (c) Goodin, D. B.; Yachandra, V. K.; Britt, R. D.; Sauer, K.; Klein, M. P. *Biochim. Biophys. Acta* **1984**, *767*, 209.
(17) George, G. N.; Prince, R. C.; Cramer, S. P. *Science* **1989**, *243*, 789.
(18) Guiles, R. D.; Zimmermann, J.-L.; McDermott, A. E.; Yachandra, V. K.; Cole, J. L.; Dexheimer, S. L.; Britt, R. D.; Wieghardt, K.; Bossek, U.; Sauer, K.; Klein, M. P. *Biochemistry*, in press.

Table VII. Summary of Geometrical Parameters

	I[a]		II[b]
	X-ray	EXAFS	EXAFS
Fe–Fe,[c] Å	3.33	3.30	3.36
Fe–Fe,[d] Å	3.53	3.53	3.55
Fe–O,[c] Å	1.82	1.80	1.82
Fe–O,[d] Å	2.00	1.99	2.01
Fe–N, Å	2.22	2.20	2.22
Fe–O–Fe,[c] deg	132.6	132.9	134.8
Fe–O–Fe,[d] deg	124.5	125.0	124.0

[a] $[L_4Fe_4(\mu\text{-}O)_2(\mu\text{-}OH)_4]I_4\cdot 3H_2O$. [b] $[L_4Fe_4(\mu\text{-}O)_2(\mu\text{-}OH)_4](ClO_4)_4\cdot 3H_2O$. [c] O bridge. [d] OH bridge.

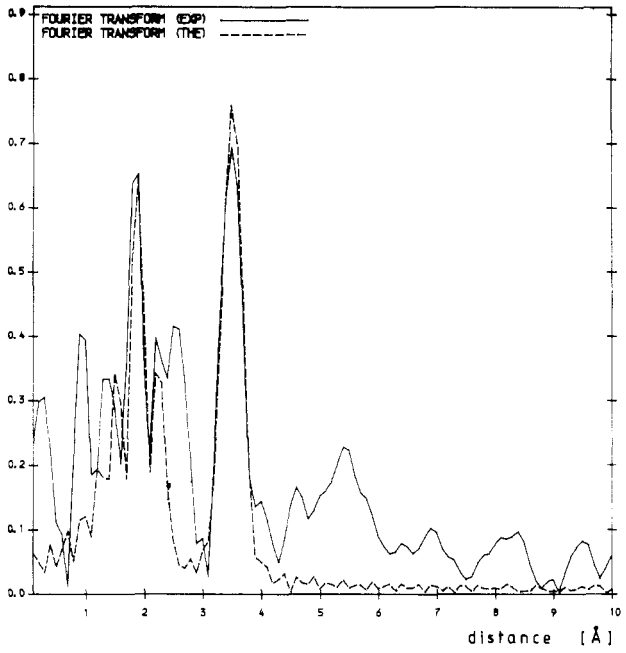

Figure 3. Fourier-transformed experimental and theoretical EXAFS spectra for $[L_4Fe_4(\mu\text{-}O)_2(\mu\text{-}OH)_4]I_4\cdot 3H_2O$.

the present $[L_4Fe_4(\mu\text{-}O)_2(\mu\text{-}OH)_4]^{4+}$ species was considered to be an ideal candidate.

Two questions were of primary interest: (1) Do EXAFS spectra allow us to distinguish between the two different Fe···Fe distances (Table III) in the region (3.1–3.9 Å)? (2) The Fe–O_{oxo} and Fe–$O_{hydroxo}$ bond distances differ by 0.18 Å. Does the fitting of the EXAFS spectra reproduce this difference accurately?

The analysis of the EXAFS data was performed by using the EXCURV program based on a curved-wave formalism.[19] Two regions (1.45–2.2 and 3.1–3.9 Å) were isolated from the EXAFS spectrum by means of a Fourier filtering technique and were fitted separately in order to obtain an initial set of fit parameters. The short-distance region includes as nearest neighbors O_{oxo}, $O_{hydroxo}$, and N shells, whereas the long-distance region includes as next-nearest neighbors Fe shells. The final fit of EXAFS parameters was performed on the unfiltered experimental EXAFS spectrum. The actual number of each kind of atom (O, N, or Fe) within the shells was kept constant at values based on the

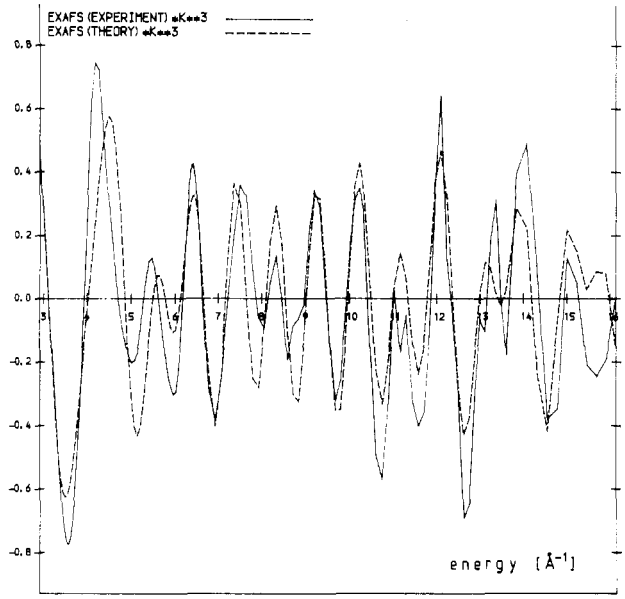

Figure 4. Experimental EXAFS spectrum for $[L_4Fe_4(\mu\text{-}O)_2(\mu\text{-}OH)_4](ClO_4)_4\cdot 3H_2O$ and fit curve obtained with the parameters listed in Table VI. The deviation of experiment and theory is due to the fact that the theoretical spectrum represents the two regions 1.45–2.2 and 3.1–3.9 Å of the Fourier transform only.

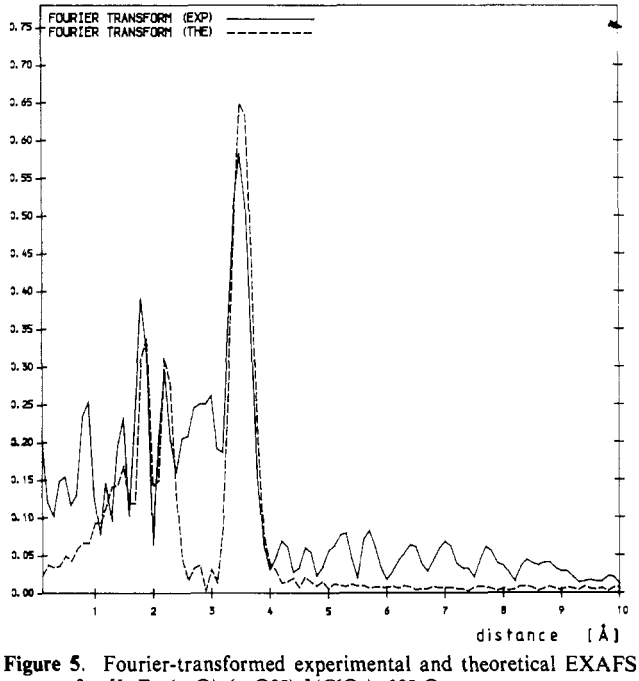

Figure 5. Fourier-transformed experimental and theoretical EXAFS spectra for $[L_4Fe_4(\mu\text{-}O)_2(\mu\text{-}OH)_4](ClO_4)_4\cdot 3H_2O$.

crystal structure of the $[L_4Fe_4(\mu\text{-}O)_2(\mu\text{-}OH)_4]^{4+}$ cation; otherwise, the obtained numbers of atoms deviate by approximately ±1 from the expected values. The results are presented in Table VI, and the experimental and theoretical spectra as well as their Fourier transforms are shown in Figures 2–5. Table VII gives a comparison of distances obtained from the X-ray structure analysis and EXAFS spectroscopy.

The EXAFS data clearly show that both the tetraiodide and tetraperchlorate salts contain the same $[L_4Fe_4(\mu\text{-}O)_2(\mu\text{-}OH)_4]^{4+}$ cations. Two different Fe···Fe distances within the adamantane-like core are discernible, and their values agree excellently with those determined by single-crystal X-ray crystallography. Most gratifyingly, the Fe–O_{oxo}, Fe–$O_{hydroxo}$, and Fe–N bond distances are also identical within experimental uncertainties. Even the differing Fe–O–Fe and Fe–OH–Fe bond angles are accurately reproduced by the fit of the EXAFS spectra. Thus, this study demonstrates convincingly that EXAFS spectra of quite com-

(19) Gurman, S. J.; Binsted, N.; Ross, I. *J. Phys.* **1984**, *C17*, 143; **1986**, *C19*, 1845.
(20) All computations were carried out on an Eclipse computer using the SHELXTL program package.
(21) *International Tables for X-Ray Crystallography*; Kynoch: Birmingham, England, 1974; Vol. IV, pp 99, 149.
(22) Stewart, R. F.; Davidson, E. R.; Simpson, W. T. *J. Chem. Phys.* **1965**, *42*, 3175.
(23) Hermes, C.; Gilberg, E.; Koch, M. H. J. *Nucl. Instrum. Methods Phys. Res. A* **1984**, *222*, 207.
(24) (a) Murray, K. S. *Coord. Chem. Rev.* **1974**, *12*, 1. (b) Gibb, T. C.; Greenwood, N. N. In *Mössbauer Spectroscopy*; Chapman and Hall: London, 1971; pp 148–164.
(25) Jeske, W.; Wieghardt, K. Unpublished results.

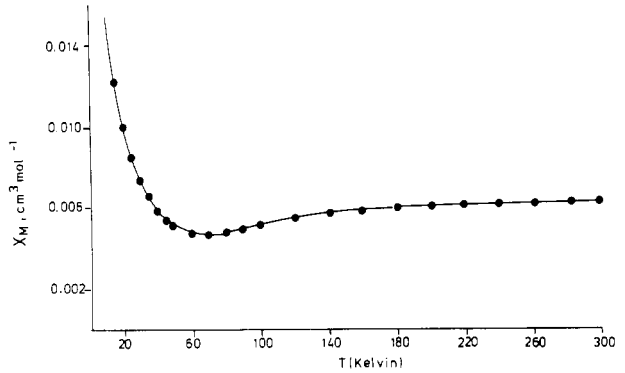

Figure 6. Molar magnetic susceptibility of $[L_4Fe_4(\mu\text{-}O)_2(\mu\text{-}OH)_4]I_4 \cdot 3H_2O$ as a function of the temperature.

Chart I

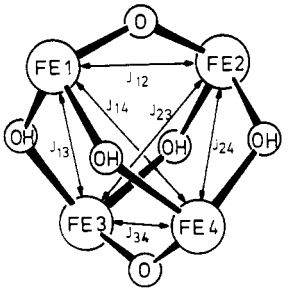

plicated polynuclear coordination compounds give reliable results. It also emphasizes—once again—that the correct model compound which reproduces all the known EXAFS features of the active site in photosystem II has yet to be prepared by inorganic chemists.

Magnetism and Mössbauer Spectrum. The magnetic moment of $[L_4Fe_4(\mu\text{-}O)_2(\mu\text{-}OH)_4]I_4 \cdot 3H_2O$ is 1.94 μ_B/Fe(III) at 299.4 K and 0.35 μ_B/Fe(III) at 2.1 K, in good agreement with values reported for Que's complex.[10] This behavior indicates strong intramolecular antiferromagnetic coupling of the high-spin ferric ions via the oxo and hydroxo bridges. The ground state of the tetranuclear cation is diamagnetic ($S = 0$), as is derived from the χ_M vs T plot shown in Figure 6. There is a maximum of six exchange coupling constants in the tetranuclear complex, which are defined in Chart I. Due to the presence of only two types of bridging ligands, and due to the symmetry of the unsymmetrical adamantane-like core, these reduce to only two different exchange coupling constants, where J represents the exchange coupling via the oxo bridges and J' via the hydroxo bridges. Hence, the isotropic exchange Hamiltonian takes the form

$$H = -[2J(\hat{S}_1 \cdot \hat{S}_2 + \hat{S}_3 \cdot \hat{S}_4) + 2J'(\hat{S}_1 \cdot \hat{S}_3 + \hat{S}_1 \cdot \hat{S}_4 + \hat{S}_2 \cdot \hat{S}_3 + \hat{S}_2 \cdot \hat{S}_4)] \quad (3)$$

where

$$S_i = 5/2 \qquad i = 1\text{-}4$$

For binuclear oxo- and hydroxo-bridged high-spin Fe(III) complexes the exchange coupling via the oxo bridges is stronger than that via the hydroxo bridges. Thus, the relation $|J| > |J'|$ has been assumed to hold in the present case and the intramolecular coupling was treated by the molecular field approximation.[26]

The molar paramagnetic susceptibility was then readily fitted to the expression given in

$$\chi_M = \frac{nNg^2\beta^2[F(J,T)]}{k(T - 2zJ'[F(J,T)])} + \text{PAR} \cdot S \cdot (S+1)\frac{Ng^2\beta^2}{3kT} + \text{TIP} \quad (4)$$

(26) Hatfield, W. E. *Theory and Applications of Molecular Paramagnetism*; Boudreaux, E. A., Mulay, L. N., Eds.; Wiley: New York, 1976; pp 491–495.

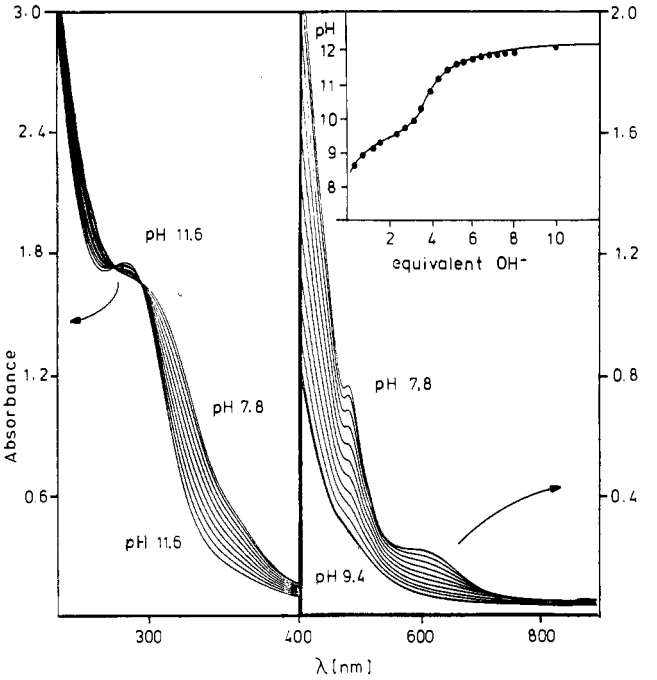

Figure 7. UV–vis spectra of $[L_4Fe_4(\mu\text{-}O)(\mu\text{-}OH)_4](ClO_4)_4 \cdot 3H_2O$ as a function of pH in aqueous sodium borate–NaOH buffer solutions (left-hand side, $[Fe_4] = 1.4 \times 10^{-4}$ M; right-hand side, $[Fe_4] = 1.4 \times 10^{-3}$ M; 1-cm quartz cell). The inset shows a titration curve ($[Fe_4] = 1.4 \times 10^{-3}$ M, 0.1 M NaOH, $I = 0.1$ M).

where n is the number of dimeric subunits within the tetramer ($n = 2$), z' is the number of neighboring dimers within the tetramer ($z' = 1$), and $F(J,T)$ is defined as

$$F(J,T) = [2\exp(A) + 10\exp(B) + 28\exp(C) + 60\exp(D) + 110\exp(E)]/[1 + 3\exp(A) + 5\exp(B) + 7\exp(C) + 9\exp(D) + 11\exp(E)] \quad (5)$$

where $A = 2J/kT$, $B = 6J/kT$, $C = 12J/kT$, $D = 20J/kT$, and $E = 30J/kT$. The second term in eq 4 accounts for the spin-only magnetism associated with a paramagnetic impurity of molar fraction (PAR) and spin S, and the last term (TIP) represents the temperature-independent paramagnetism (and diamagnetism), which is set equal to zero in the fit procedure. A least-squares fit yielded $g = 2.06$, $J = -106.3$ (2) cm^{-1}, $J' = -15.1$ (2) cm^{-1}, PAR = 0.064, and $S = 5/2$. These values agree qualitatively with those reported for Schugar's tetranuclear complex $Na_6[Fe_4L_2(\mu\text{-}O)_2(\mu\text{-}CO_3)_2]$, where L represents the deprotonated form of [(2-hydroxo-1,3-propanediyl)diimino]tetraacetic acid. This complex may also be envisaged as a dimer of the binuclear (μ-oxo)(μ-carbonato)diiron core. This formal dimer formation is achieved by two alkoxo bridges. A J value for intramolecular antiferromagnetic coupling across the [Fe–O–Fe] unit of −63.4 cm^{-1} and a $z'J'$ value for intramolecular coupling across the alkoxo bridges of −11.2 cm^{-1} have been reported.[11a] Since the two dimers in the Schugar complex are connected by two alkoxo bridges, the value of z' is 1/2 and consequently J' is −22.4 cm^{-1}.

The Mössbauer spectra of $[L_4Fe_4(\mu\text{-}O)_2(\mu\text{-}OH)_4]I_4 \cdot 3H_2O$ at 4.2 K (external field of 200 G) and at 77 K (zero field) consist of a symmetric quadrupole doublet. Isomer shifts, δ, were 0.46 (2) mm/s at 4.2 K and 0.45 (2) mm/s at 77 K; quadrupole splittings, ΔE_Q, of 1.37 (1) and 1.33 (1) mm/s at 4.2 and 77 K, respectively, were observed. The line widths (full width at half-maximum) of 0.25 and 0.37 mm/s at 4.2 and 77 K, respectively, are consistent with four equivalent iron sites. The isomer shift is well within the range ($0.3 < \delta < 0.6$ mm/s) observed for a wide variety of monomeric and oxo-bridged high-spin ferric complexes.[24]

Solution Behavior. The tetranuclear cation displays interesting solution behavior. Titration of a 1.4×10^{-3} M aqueous solution (0.1 M $NaClO_4$) of the perchlorate salt with 0.1 M NaOH revealed that 2 equiv of base and then a further 2 equiv are con-

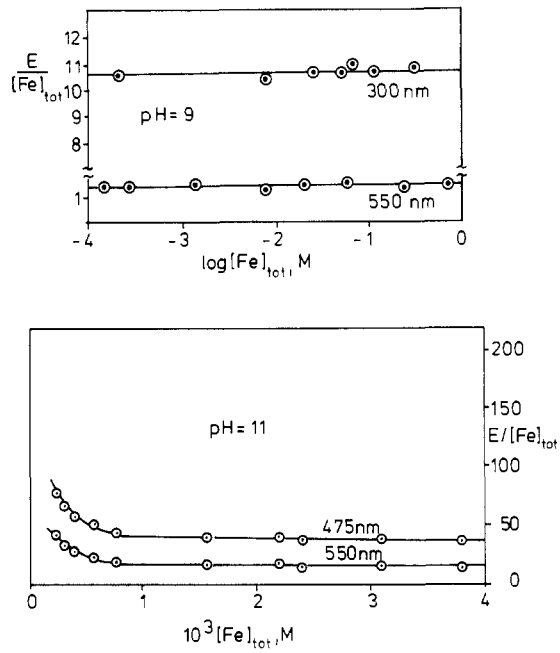

Figure 8. Dependence of the absorbance, $E/[Fe]_{tot}$, at two different wavelengths, on the total ferric concentration, $[Fe]_{tot}$, at constant pH: (top) pH = 9, buffer borate–HCl; (bottom) pH = 11, buffer glycine–NaOH–NaCl.

sumed. This process is completely reversible; reacidification of the basic solution yielded the same pH-titration curve (see inset of Figure 7). It is conceivable that the four μ-hydroxo bridges in $[L_4Fe_4O_2(OH)_4]^{4+}$ are deprotonated in two consecutive steps, generating the neutral complex $[L_4Fe_4O_6]^0$ via the $[L_4Fe_4(O)_4(\mu\text{-}OH)_2]^{2+}$ species.

An alternative model involves the cleavage of the adamantane $[Fe_4(O)_2(OH)_4]^{4+}$ core A via addition of two OH^- ligands, generating species B, and finally, after addition of two further OH^- ligands, the tetramer is cleaved, forming the dimer C. For the

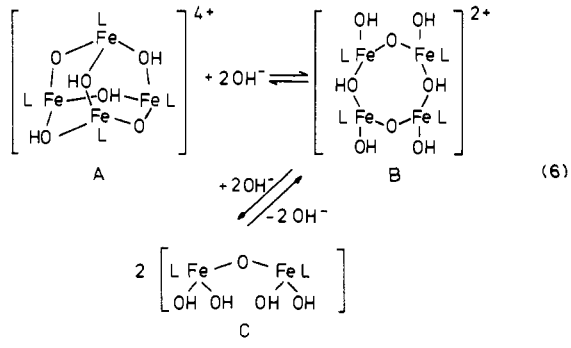

(6)

reaction sequence (6) equilibria may then be formulated as shown in eq 7 and 8. From the pH-titration curve shown in the inset

$$A + 2OH^- \rightleftharpoons B \qquad K_1 = \frac{[B]}{[A][OH^-]^2} \tag{7}$$

$$B + 2OH^- \rightleftharpoons 2C \qquad K_2 = \frac{[C]^2}{[B][OH^-]^2} \tag{8}$$

of Figure 7, it is clear that in the pH range 7–9.5 species A and B are predominantly in equilibrium. Thus, in a buffer solution at pH 9.0 the total ferric concentration is given by the sum of the concentrations of species A and B. Upon variation of $[Fe]_{tot}$ at constant pH = 9.0 the ratio [A]/[B] does not change (eq 7) and, consequently, Beer's law for the absorbance changes in the UV–vis spectrum should hold at any wavelength. This is observed as shown in Figure 8. On the other hand, at pH > 10 $[Fe]_{tot}$ is given by the sum of [B] and [C]. At constant pH = 11 variation of $[Fe]_{tot}$ leads to ratios of [C]/[B] that depend on $[Fe]_{tot}$ (eq 8) and, therefore, Beer's law does not hold. This has also been observed (Figure 8). These observations are consistent with the proposed scheme (eq 6) and not with simple protonation–deprotonation reactions of a tetranuclear species.

We have as yet not been able to isolate and characterize species B or C, but it is noted that dimers of type C, $[L_2Fe_2(\mu\text{-}O)X_4]$, where X represents N_3^- or Cl^-, have been isolated. The tetrachloro dimer dimerizes indeed in basic aqueous solution, forming A.[25] Similar complex equilibria have been proposed for Que's tetramer.[10]

Experimental Section

The complexes $[L_2Fe_2(acac)_2(\mu\text{-}O)](ClO_4)_2$ and $LFeCl_3$ have been prepared as described previously.[6]

$[L_4Fe_4(\mu\text{-}O)_2(\mu\text{-}OH)_4]X_4\cdot 3H_2O$ (X = I, ClO_4). Method A. NaI or alternatively, $NaClO_4\cdot H_2O$ (1 g) was added to a solution of $[L_2Fe_2(acac)_2(\mu\text{-}O)](ClO_4)_2$ (0.10 g 0.12 mmol) in an acetone–water mixture (1:1; 50 mL). The solution was allowed to stand in an open vessel for 2 weeks, after which time green microcrystals had precipitated from the green solution, which were filtered off, washed with ethanol and ether, and air-dried (yield ~30%).

Single crystals of the tetraiodide suitable for X-ray crystallography were grown by slow diffusion of an aqueous solution of NaI into a solution containing the crude tetraiodide salt.

Method B. A solution of $LFeCl_3$ (0.25 g) in water (20 mL) to which pyridine (2 mL) was added was stirred at room temperature for 15 min. To the clear green solution was added $NaClO_4$ (3 g) or NaI (1 g). Green microcrystals precipitated, which were filtered off. Anal. Calcd for $[(C_6H_{15}N_3)_4Fe_4O_2(OH)_4]I_4\cdot 3H_2O$: C, 20.55; H, 5.00; N, 11.99; Fe, 15.89. Found: C, 20.5; H, 4.9; N, 12.0; Fe, 14.6. Calcd for $[(C_6H_{15}N_3)_4Fe_4O_2(OH)_4](ClO_4)_4\cdot 3H_2O$: C, 22.30; H, 5.42; N, 13.01; Fe, 17.24. Found: C, 22.2; H, 5.6; N, 13.1; Fe, 18.1.

X-ray Crystallography. A green-black irregularly shaped crystal of $[L_4Fe_4(\mu\text{-}O)_2(\mu\text{-}OH)_4]I_4\cdot 3H_2O$ was attached to a glass fiber and mounted on a four-circle Syntex R3 diffractometer. The unit cell dimensions were obtained by a least-squares fit to the setting angles of 25 reflections ($4 < 2\theta < 25°$). The data are summarized in Table I. Intensity data were corrected for Lorentz and polarization effects in the usual manner; an empirical absorption correction (ψ scans of seven reflections; $6 < 2\theta < 42°$) was also carried out.[20] The structure was solved via conventional Patterson and difference Fourier syntheses. Neutral-atom scattering factors and anomalous dispersion corrections for non-hydrogen atoms were taken from ref 21 and hydrogen atom scattering factors from ref 22. The positions of the methylene and amine hydrogen atoms were calculated (d(C–H) = d(N–H) = 0.96 Å; sp^3-hybridized carbon or nitrogen) and were included in the final refinement cycle with isotropic thermal parameters. H atoms of water molecules of crystallization were not located. All non-hydrogen atoms were refined with use of anisotropic displacement parameters. The function minimized during least-squares refinement was $\sum w(|F_o| - |F_c|)^2$, where $w = 1/\sigma^2(F)$. Final atom coordinates are listed in Table II.

EXAFS Spectroscopy. X-ray absorption spectra were recorded in the absorption mode at the EXAFS measuring stand of EMBL Outstation at Deutsches-Elektronen-Synchrotron in Hamburg, FRG. The experimental setup is described in ref 23. The Si(111) double crystal was used as the monochromator. All data were collected at 20 K. EXAFS data reduction and background removal were done in the standard manner.[27]

Physical Measurements. Electronic spectra were recorded with quartz cuvettes on a Perkin-Elmer Lambda 9 spectrophotometer. The variable-temperature magnetic susceptibility of a powdered sample of $[L_4Fe_4(\mu\text{-}O)_2(\mu\text{-}OH)_4]I_4\cdot 3H_2O$ was measured by the Faraday method in the range 4–300 K. Diamagnetic corrections were applied in the usual manner with use of Pascal's constants. Mössbauer measurements were performed with a conventional setup in the constant-acceleration mode with use of a 50-mCi $^{57}Co/Rh$ source. The spectra were analyzed by a least-squares fit procedure with use of a Lorentzian line shape, and calibration was achieved with respect to α-Fe at ambient temperature.

Acknowledgment. We thank the Fonds der Chemischen Industrie and the Bundesministerium für Forschung und Technologie for financial support of this work. We are grateful to Prof. Dr. P. Gütlich (Mainz, FRG) for the temperature-dependent sus-

(27) Teo, B. K. *EXAFS: Basic Principles and Data Analysis*; Springer-Verlag: West Berlin, 1986.
(28) Joyner, R. W.; Martin, K. J.; Mechan, P. *J. Phys. C.* **1987**, *20*, 4005.

ceptibility measurements. We thank Dr. C. Hermes (EMBL Outstation, Hamburg, FRG) for measuring the EXAFS spectra.

Registry No. $[L_4Fe_4(\mu\text{-}O)_2(\mu\text{-}OH)_4]I_4\cdot 3H_2O$, 123567-48-6; $[L_4Fe_4(\mu\text{-}O)_2(\mu\text{-}OH)_4](ClO_4)_4\cdot 3H_2O$, 123567-50-0; $[L_2Fe_2(acac)_2(\mu\text{-}O)](ClO_4)_2$, 118486-84-3; $LFeCl_3$, 86823-88-3.

Supplementary Material Available: Tables of complete crystallographic data, bond distances and angles, and thermal parameters (5 pages); a listing of structure factor amplitudes (43 pages). Ordering information is given on any current masthead page.

Contribution from the Department of Chemistry and Biochemistry, Utah State University, Logan, Utah 84322-0300, and Department of Chemistry, University of Arizona, Tucson, Arizona 85721

Molybdenum(VI)–Dioxo Complexes with Linear and Tripodal Tetradentate Ligands: Models for the Molybdenum(VI/V) Centers of the Molybdenum Hydroxylases and Related Enzymes. 1. Syntheses and Structures

Carol J. Hinshaw,[1a] Gang Peng,[1a] Raghuvir Singh,[1a] Jack T. Spence,*[,1a] John H. Enemark,[1b] Michael Bruck,[1b] John Kristofzski,[1b] Shannath L. Merbs,[1b] Richard B. Ortega,[1b] and Pamela A. Wexler[1b]

Received January 12, 1989

As models for the molybdenum(VI/V) centers of the molybdenum hydroxylases and related enzymes, 15 new Mo(VI)–dioxo complexes (MoO_2L) with tetradentate ligands have been synthesized and characterized. The effects of coordinating groups (N_2S_2, N_2OS, and N_2O_2), chelate ring size (five and six members), ligand geometry (linear and tripodal), and steric bulk have been investigated. X-ray crystal structures have been obtained for seven of the complexes. While minor differences, attributed to these features, are evident, the structures have remarkably similar Mo–ligand bond lengths and bond angles and all have distorted-octahedral geometry. The oxo groups are cis to one another and to the thiolate or phenolate groups of the ligands. The N atoms are approximately trans to the oxo groups, and the Mo—N bonds are relatively long (>2.34 Å), with the bond length correlated with the size of the trans O=Mo—N bond angle. The Mo=O and Mo—S(thiolate) bond lengths are comparable to those determined by EXAFS spectroscopy for the Mo centers of the enzymes. The relevance of the results to the structures of the Mo centers of the enzymes is discussed.

Introduction

The molybdenum hydroxylases and related enzymes catalyze two-electron-redox processes in which an oxygen atom or a hydroxyl group is added to or removed from the substrate. The most extensively studied of these enzymes are xanthine oxidase (XO),[2a] xanthine dehydrogenase (XDH),[3a] sulfite oxidase (SO),[2a] and nitrate reductase (NR).[2b] The minimal structure of the molybdenum center, as deduced by EXAFS and EPR investigations, for oxidized XO and XDH is $Mo^{VI}O(S)(SR)_2$.[3] A $Mo^{VI}O_2(SR)_{2-3}$ center appears to be present in oxidized SO and NR from *Chlorella vulgaris*.[3a] Some of the thiolate (SR) ligands are probably furnished by the cofactor, Mo-co,[4] and additional oxygen, nitrogen, or thioether ligands may also be present.[3]

The enzyme molybdenum centers cycle between the VI, V, and IV oxidation states during catalysis.[2] The Mo centers undergo reversible reduction, and in most cases, the potentials are pH and anion dependent.[5] Two-electron reduction has been interpreted as generating (omitting SR ligands) $Mo^{IV}O(SH)$ (XO, XDH)[2,3] or $Mo^{IV}O(OH)$ (SO, NR)[2,3] centers that, upon one-electron reoxidation, give EPR signals which have been interpreted as arising from $Mo^{V}OS$,[3d] $Mo^{V}O(SH)$,[3a,b] and $Mo^{V}O(OH)$[2b,3,6-8] centers.

In contrast to the behavior of the enzyme Mo centers, most Mo(VI)–dioxo complexes undergo irreversible electrochemical reduction, with formation of oxo-bridged dimers[9a] or with deprotonation of amino ligands and loss of an oxo ligand as H_2O.[9b] Recent reports[10-12] indicate these biomimetically undesirable results may be avoided by proper ligand design. Specifically, tetradentate N_2S_2 and N_2O_2 ligands (L) with alkylated (tertiary) nitrogen atoms have been shown to give Mo(VI)–dioxo complexes (MoO_2L) that are reported to undergo reversible one-electron reduction and to stabilize $[Mo^{V}O_2L]^-$, $[Mo^{V}O(S)L]^-$, *cis*-$Mo^{V}O(OH)L$, and *cis*-$Mo^{V}O(SH)L$ species in solution.[11] For one such ligand, both $[Ph_4P][Mo^{V}OSL]$ and *trans*-$Mo^{V}O(SH)L$ have been isolated.[13] These results are clearly relevant for understanding the molybdenum centers of the enzymes.

We report here the syntheses of 15 new Mo(VI)–dioxo complexes with tetradentate N-alkylated ligands in which the effects of coordinating groups (N_2O_2, N_2OS, N_2S_2), chelate ring size (five and six members), ligand geometry (linear and tripodal), and steric bulk have been systematically varied. The complexes have been

(1) (a) Utah State University. (b) University of Arizona.
(2) (a) Hille, R.; Massey, V. In *Molybdenum Enzymes*; Spiro, T. G., Ed.; Wiley: New York, 1985; p 443. (b) Adams, M. W. W.; Mortenson, L. E. In ref 2a, p 519.
(3) (a) Cramer, S. P. *Adv. Inorg. Bioinorg. Mech.* **1983**, *2*, 259. (b) Cramer, S. P.; Wahl, R. C.; Rajagopalan, K. V. *J. Am. Chem. Soc.* **1981**, *103*, 7721. (c) George, G. N.; Bray, R. C.; Cramer, S. P. *Biochem. Soc. Trans.* **1986**, *14*, 651. (d) Bray, R. C.; George, G. N. *Biochem. Soc. Trans.* **1985**, *13*, 560. (e) Bray, R. C.; Gutteridge, S.; Storter, D. A.; Tanner, S. J. *Biochem. J.* **1979**, *177*, 357.
(4) Johnson, J. L.; Hainline, B. E.; Rajagopalan, K. V.; Arison, B. H. *J. Biol. Chem.* **1984**, *259*, 5414. Hawkes, T. R.; Bray, R. C. *Biochem. J.* **1984**, *219*, 481. Cramer, S. P.; Stiefel, E. I. In *Molybdenum Enzymes*; Spiro, T. E., Ed.; Wiley: New York, 1985; p 411.
(5) Spence, J. T.; Kipke, C. A.; Enemark, J. H.; Sunde, R. A. Submitted for publication.
(6) (a) Bray, R. C. *Adv. Enzymol. Relat. Areas Mol. Biol.* **1980**, *51*, 107. (b) George, G. N.; Bray, R. C. *Biochemistry* **1988**, *27*, 3603.
(7) (a) Bray, R. C. In *Biological Magnetic Resonance*; Berliner, L. J., Reuben, J., Eds.; Plenum Press: New York, 1980; Vol. 2, p 45. (b) Bray, R. C.; Gutteridge, S.; Lamy, M. T.; Wilkinson, T. *Biochem. J.* **1983**, *211*, 227. (c) Gutteridge, S.; Bray, R. C.; Nottom, B. A.; Fido, R. J.; Hewitt, E. J. *Biochem. J.* **1983**, *213*, 137. (d) Vincent, S. P.; Bray, R. C. *Biochem. J.* **1978**, *171*, 639.
(8) Solomonson, L. P.; Barker, M. J.; Howard, W. D.; Johnson, J. L.; Rajagopalan, K. V. *J. Biol. Chem.* **1984**, *259*, 849.
(9) (a) Stiefel, E. I. *Prog. Inorg. Chem.* **1977**, *22*, 1. (b) Subramanian, P.; Spence, J. T.; Ortega, R. B.; Enemark, J. H. *Inorg. Chem.* **1984**, *23*, 2564. Rajan, O. R.; Spence, J. T.; Leman, C.; Minelli, M.; Sato, M.; Enemark, J. H.; Kroneck, P. M. H.; Sulger, K. *Inorg. Chem.* **1983**, *22*, 3065.
(10) Hinshaw, C. J.; Spence, J. T. *Inorg. Chim. Acta* **1986**, *125*, L17.
(11) Dowerah, D.; Spence, J. T.; Singh, R.; Wedd, A. G.; Wilson, G. L.; Farchione, F.; Enemark, J. H.; Kristofzski, J.; Bruck, M. *J. Am. Chem. Soc.* **1987**, *109*, 5655.
(12) Farchione, F.; Hanson, G. R.; Rodrigues, C. G.; Bailey, T. D.; Bajchi, R. N.; Bond, A. M.; Pilbrow, J. R.; Wedd, A. G. *J. Am. Chem. Soc.* **1986**, *108*, 831.
(13) Singh, R.; Spence, J. T.; Cramer, S. P.; George, G. N. *Inorg. Chem.* **1989**, *28*, 8.

0020-1669/89/1328-4483$01.50/0